1   **The Response of Tropical Tropospheric Ozone to ENSO**
2
3
4   L. D. Oman[1], J. R. Ziemke[1,2], A. R. Douglass[1], D. W. Waugh[3],
5   C. Lang[3], J. M. Rodriguez[1], J. E. Nielsen[1,4]
6
7   *[1]NASA Goddard Space Flight Center, Greenbelt, MD, USA; [2]University of Maryland Baltimore*
8   *County, Baltimore, MD, USA; [3]Johns Hopkins University, Baltimore, MD, USA; [4]Science Systems*
9   *and Applications Inc., Lanham, MD, USA*
10
11
12
13
14
15
16
17
18   Submitted to GRL
19   May 2011
20
21
22
23
24
25
26
27
28
29
30
31
32
33
34
35
36
37
38
39   *Corresponding Author:*
40   Luke D. Oman
41   NASA Goddard Space Flight Center
42   Atmospheric Chemistry and Dynamics Branch
43   Code 613.3
44   Greenbelt, MD 20771
45   *E-mail:* luke.d.oman@nasa.gov
46

47   **Abstract**

48   We have successfully reproduced the Ozone ENSO Index (OEI) in the Goddard Earth

49   Observing System (GEOS) chemistry-climate model (CCM) forced by observed sea surface

50   temperatures over a 25-year period. The vertical ozone response to ENSO is consistent

51   with changes in the Walker circulation. We derive the sensitivity of simulated ozone to

52   ENSO variations using linear regression analysis. The western Pacific and Indian Ocean

53   region shows similar positive ozone sensitivities from the surface to the upper

54   troposphere, in response to positive anomalies in the Niño 3.4 Index. The eastern and

55   central Pacific region shows negative sensitivities with the largest sensitivity in the upper

56   troposphere. This vertical response compares well with that derived from SHADOZ

57   ozonesondes in each region. The OEI reveals a response of tropospheric ozone to

58   circulation change that is nearly independent of changes in emissions and thus it is

59   potentially useful in chemistry-climate model evaluation.

60

61   **Introduction**

62   The El Niño-Southern Oscillation (ENSO) is the dominant mode of tropical

63   variability on interannual timescales [*Philander*, 1989]. ENSO has been long known to

64   cause significant perturbations to the coupled oceanic and atmospheric circulations

65   [*Bjerknes,* 1969; *Enfield*, 1989]. Changes in sea surface temperatures in the Pacific Ocean

66   can notably impact the Walker Circulation, displacing areas of convective activity, and have

67   also been shown to dominate the interannual variability of the Hadley cell [*Quan*, 2004].

68   These changes in circulation cause changes in the temperature and moisture fields across

69   the tropical Pacific, and influence the constituent distributions in the troposphere [*Chandra*

70 *et al.*, 1998; 2002; 2009; *Sudo and Takahashi*, 2001; *Ziemke et al.*, 2003; *Zeng and Pyle*,

71 2005; *Doherty et al.*, 2006; *Lee et al.*, 2010; *Randel and Thompson*, 2011] and in the

72 stratosphere [*Randel and Cobb*, 1994].

73 *Ziemke et al.* [2010] used tropospheric column ozone (TCO) measurements to show

74 that the ENSO related response of tropospheric ozone over the western and eastern Pacific

75 dominated interannual variability. The ENSO impact is so clearly seen in tropospheric

76 ozone columns that an Ozone ENSO Index (OEI) that largely mimics the Niño 3.4 Index is

77 formed by subtracting the eastern and central tropical Pacific region TCO (15°S-15°N,

78 110°W-180°W) from the western tropical Pacific-Indian Ocean region (15°S-15°N, 70°E-

79 140°E), removing the seasonal cycle and smoothing with a 3-month running average.

80 *Ziemke et al.* [2010] suggested that chemistry-climate models forced with observed sea

81 surface temperatures should reproduce this observed pattern in tropospheric ozone. Here

82 we will show that in the GEOS CCM tropical tropospheric ozone responds to the

83 perturbation in atmospheric dynamics that is due to the ENSO signature in tropical SSTs.

84 In addition, we use the Southern Hemisphere Additional Ozonesondes (SHADOZ)

85 measurements to evaluate the vertical structure of the simulated response to ENSO.

86

87 **Model Simulation and Measurements**

88 We examine the response of simulated tropospheric ozone to the observed sea

89 surface temperature changes using the Goddard Earth Observing System (GEOS) version 5

90 general circulation model [*Rienecker et al.*, 2008] coupled to the comprehensive Global

91 Modeling Initiative (GMI) stratosphere-troposphere chemical mechanism [*Duncan et al.*,

92 2007; *Strahan et al.*, 2007]. The GMI combined stratosphere-troposphere chemistry

93   mechanism includes 117 species, 322 chemical reactions, and 81 photolysis reactions.

94   Integration of the chemical mass balance equations use the SMVGEAR II algorithm

95   described in *Jacobson* (1995). The mechanism includes a detailed description of O_3-NO_x-

96   hydrocarbon chemistry necessary for the troposphere (*Bey et al.*, 2001), with more recent

97   updates described in *Duncan et al.* (2007). The simulation used in this study was forced

98   with observed sea surface temperatures and sea ice concentrations from 1985 to 2009

99   (*Rayner et al.*, 2003, updated on a monthly basis), but the seasonally-varying mixing ratio

100   boundary conditions and emissions for trace gases are for 2005 conditions. The simulation

101   produces the variability in constituent distributions due to sea surface temperature

102   changes that we evaluate here.

103   A record of TCO for the 2005 – 2010 period was derived from the combination of

104   NASA's Aura satellite Ozone Monitoring Instrument (OMI) and the Microwave Limb

105   Sounder (MLS) using the method described in *Ziemke et al.* [2006]. These TCO values

106   extend the time series developed using Nimbus 7 TOMS, Earth Probe TOMS and NOAA

107   SBUV. The TCO measurements for 2005 – 2010 are used in Figure 1a. A complete

108   description of the methods used to construct the OEI can be found in *Ziemke et al.* [2010].

109   Here we use the index derived from TCO measurements for 1985 - 2009 to match the

110   simulation. The OEI time series begins in 1979 and is updated periodically. The data can

111   be obtained from the Goddard tropospheric ozone website at http://toms.gsfc.nasa.gov.

112   We use ozonesonde measurements from five SHADOZ stations [*Thompson et al.*,

113   2003] (http:/croc.gsfc.nasa.gov/shadoz): two in the western region (Java and Kuala

114   Lumpur) and three in the eastern region (American Samoa, Hilo, and San Cristobal). The

115   data for Watukosek, Java (7.6°S, 112.7°E), Kuala Lumpur, Malaysia (2.7°N, 101.7°E), Pago

116   Pago, American Samoa (14.2°S, 170.6°W), and Hilo, Hawaii (19.4°N, 155.0°W) cover the

117   1998 to 2009 time period, whereas the San Cristobal (0.9°S, 89.6°W) record is slightly

118   shorter, covering 1998 to 2008.

119   We used the ENSO index based on the Niño 3.4 region and available from the NOAA

120   sea-surface temperature website (http://www.cpc.ncep.noaa.gov/data/indices/), also

121   used by *Ziemke et al.* [2010].

122

123   **Results and Discussion**

124   *Ziemke et al.* [2010] used a combination of satellite observations and simulations to

125   show that the observed tropical longitudinal structure in total column ozone was due

126   almost entirely to structure in the TCO. They identified a dipole in tropical TCO between

127   the western Pacific-Indian Ocean region and eastern and central Pacific region (15°S-15°N,

128   70°E-140°E, and 15°S-15°N, 110°W-180°W, respectively). The difference between the

129   mean TCO in these two regions, shown as black rectangles on Figure 1, is called the Ozone

130   ENSO Index (OEI). Also shown in Figure 1 is the TCO response to the Niño 3.4 Index

131   computed using linear regression analysis for both measurements and the GEOS chemistry-

132   climate model (CCM) simulation. Regression of the TCO against Niño 3.4 Index yields a

133   sensitivity coefficient or slope (DU/K) that represents the TCO change congruent with a 1K

134   increase in the Niño 3.4 Index. For reference, a typical El Niño/La Nina cycle represents

135   about a 3K range with about a 5K range for a more extreme cycle. OMI/MLS derived TCO

136   measurements [*Ziemke et al.,* 2006] for the 6 years covering 2005 to 2010 are used to

137   calculate the sensitivity coefficient (DU/K) in Figure 1a. Significant positive TCO

138   sensitivities are located throughout the western region with significant negative TCO

139   sensitivities over the eastern region. Shaded regions show sensitivities that are not

140   significant at the 95% level taking into account any autocorrelation of the residual. Figure

141   1b shows a similar 6-year period (in this case 2004 to 2009) from GEOS CCM simulated

142   TCO. The overall pattern is similar to that derived from OMI/MLS TCO with a slightly

143   negative offset in the simulation. Over the Indonesian region, the meridional extent of the

144   positive anomalies is smaller in Figure 1b than 1a, which could partially be due to the short

145   record. Also, shown (Figure 1c) is the sensitivity calculated using 25 years of the

146   simulation (from 1985 to 2009). Another significant feature that appears in both

147   measurements and simulation is positive TCO sensitivities in the central Pacific Ocean near

148   30°S.

149   The OEI is the difference between the western region average monthly TCO and that

150   computed for the eastern region. The deseasonalized time series of OEI, smoothed with a 3-

151   month running average, is shown in Figure 2 for the measurements (black curve) and

152   simulation (red curve). The Niño 3.4 Index multiplied by 3 is shown as the blue curve.

153   There is excellent agreement between all three times series: The correlation of the

154   measurement derived OEI with ENSO is 0.84 and that of the simulation derived OEI with

155   ENSO is 0.86. During El Niño, the positive phase of ENSO, the OEI anomaly is positive,

156   corresponding to increased ozone over the western region and decreased ozone over the

157   eastern region. This can be most clearly seen during the very strong 1997-1998 El Niño

158   with an anomaly of 9 DU for OEI obtained from simulated tropospheric ozone columns

159   compared with 11 DU from observations.

160   The correspondence of observed and simulated OEI prompted us to examine the

161   vertical structure of the dynamically driven ozone changes simulated with the GEOS CCM,

162   again using linear regression analysis. Regression of the simulated tropical ozone field

163   against the Niño 3.4 Index yields a sensitivity coefficient in ppbv/K. We average tropical

164   tropospheric ozone between 15°S and 15°N and regress the deseasonalized ozone field

165   with Niño 3.4 Index at each longitude and pressure level to construct Figure 3a. Since ENSO

166   is known to produce a significant change in the Walker circulation, we overlay the anomaly

167   in the streamfunction obtained by regressing the zonal wind and vertical velocity against

168   the Niño 3.4 Index. The ozone and circulation anomalies generally have inflection points

169   just to the west of the international date line, with lower ozone values and anomalous

170   upwelling to the east and higher ozone values and anomalous downwelling to the west. The

171   Walker circulation response is seen clearly in the streamfunction anomaly, which

172   corresponds very well to the pattern of ozone sensitivity. Figure 3a shows that the

173   simulated sensitivity of ozone to the Niño 3.4 Index in the western region as defined by

174   *Ziemke et al.* [2010] is ~1 to 2 ppbv/K from the surface to the tropopause with relative

175   maxima in the upper troposphere around 60°E and in the mid-troposphere around 130°E.

176   Negative values of ozone sensitivity in the eastern region are largest in the upper

177   troposphere approaching -15 ppbv/K near the tropopause.

178   We also examine the latitude dependence of the ozone and circulation response in

179   the two key regions identified by *Ziemke et al.* [2010]. The sensitivity coefficients (ppbv/K)

180   formed from linearly regressing deseasonalized average ozone in the eastern region

181   (180°W-110°W) and western region (70°E-140°E) against the Niño 3.4 Index for each

182   latitude and altitude are given in Figures 3b and 3c respectively. Again we overlay the

183   anomalous circulation shown by the streamfunction obtained this time by regressing the

184   meridional wind and vertical velocity against the Niño 3.4 Index. The dashed black curve

185   shows the mean model tropopause in each region. In the eastern region a stronger mean

186   ascending branch of Walker circulation is seen near the equator. This simulated eastern

187   region response of the circulation is consistent with the observed rawinsonde station data

188   analyzed by *Oort and Yienger* [1996] and produces a corresponding tropospheric ozone

189   response. The region of decreased ozone generally broadens in latitude as altitude

190   increases with values from -3 ppbv/K in the equatorial mid-troposphere to -15 ppbv/K

191   near the tropical tropopause. The positive ozone anomalies with increased tropical SSTs in

192   the midlatitudes of Figure 3b could be consistent with increased stratosphere-troposphere

193   exchange of ozone. *Zeng and Pyle* [2005] also found an increase in the stratosphere-

194   troposphere exchange of ozone in their CCM simulation of the impact of ENSO. Other

195   studies suggested observational evidence for this impact in observations above Colorado

196   [*Langford et al.,* 1998; *Langford,* 1999]. The recent analysis of *Voulgarakis et al.* [2011] has

197   also simulated enhanced stratosphere-troposphere exchange of ozone following the strong

198   1997-1998 El Niño event.

199   *Chandra et al.* [1998] found that downward motion, suppressed convection, and a

200   drier troposphere contribute to the ozone increase over the tropical western Pacific and

201   Indonesian region. The combination of downward motion and suppressed convection

202   bring ozone produced in the upper troposphere down [*Sudo and Takahashi,* 2001], and

203   reduce the upward transport of low ozone air over ocean surfaces, increasing ozone values

204   in the low to mid troposphere. Additionally, the drier troposphere increases the chemical

205   lifetime of ozone, which also acts to increase tropospheric ozone concentrations [*Kley et al.,*

206   1996]. These results are consistent with the GEOS CCM simulation and are shown in Figure

207   3c by the anomalous downward component in the circulation.

208   We evaluate the simulated vertical ozone response to ENSO using data collected by

209   the SHADOZ network [*Thompson et al.*, 2003]. There are SHADOZ stations in and around

210   the two key regions shown in *Ziemke et al.* [2010]. In Figure 4 we compare the simulated

211   ENSO related vertical ozone sensitivity to that obtained using observations from two

212   western region SHADOZ locations (Java and Kuala Lumpur) and three eastern region

213   SHADOZ locations (American Samoa, Hilo, and San Cristobal) for 1998-2009. Although in

214   the eastern region only American Samoa is within the box defined by *Ziemke et al.* [2010],

215   the other two locations are just north (Hilo) and east (San Cristobal) of the region and still

216   located in the area significantly correlated with ENSO. We deseasonalized each

217   ozonesonde record prior to averaging them within each region and then regress the

218   resulting values against the Niño 3.4 Index. In the western region (red diamonds), values

219   are nearly all statistically significant and positive (2 standard deviation interval shown

220   from regression). In the eastern region (blue diamonds) SHADOZ reveals significant large

221   negative values in the upper troposphere similar to those simulated. In the low to mid

222   troposphere ozone anomalies are generally not significantly different from zero. Also,

223   plotted on Figure 4 are the ozone sensitivities from the GEOS CCM simulation (solid curves)

224   sampled at the same locations as the SHADOZ stations. In the western region the GEOS CCM

225   simulation underestimates the magnitude of the positive anomalies, while in the upper

226   troposphere of the eastern region the negative anomalies are larger than those derived

227   from SHADOZ stations. Overall these patterns in SHADOZ regional composites are similar

228   to those obtained by *Lee et al.* [2010] for two individual stations (Kuala Lumpur and San

229   Cristobal), and more recently for several stations used by *Randel and Thompson* [2011].

230

231 **Conclusions**

232   We have demonstrated that the relationship between tropical SST anomalies and

233 the response of tropical tropospheric ozone is clearly reproduced in the GEOS CCM

234 simulation forced with time varying observed SSTs. Such agreement requires both a

235 realistic response of the circulation to the SST and realistic simulated horizontal and

236 vertical ozone gradients. The OEI represents an essential physical relationship that coupled

237 chemistry-climate models should reproduce and is potentially useful in future chemistry-

238 climate model evaluations. Tropical tropospheric ozone changes appear to be congruent

239 with anomalous changes to the Walker circulation cell.

240   The impact of changes in biomass burning is not considered in this simulation.

241 Although, previous work (*e.g., Thompson et al.*, 2001) has shown its importance in ozone

242 production, time-dependent emissions are not critical for reproducing the OEI. *Ziemke et*

243 *al.* [2009] used emissions appropriate for the 2006 El Niño event; their results suggest that

244 the change in emissions accounts for no more than 20% of the OEI response. Simulations

245 indicate that ozone anomalies produced from interannual variability in biomass burning

246 are transported throughout the tropics over the 3 month averaging period that is used in

247 constructing the OEI. Only a strong local increase in one region but not the other will

248 impact the OEI.

249   This analysis demonstrates that ENSO-related changes in the circulation, thermal

250 structure and composition drive tropical ozone variability. Future work will include a

251 detailed budget analysis to determine the relative contributions of dynamical, chemical,

252 and thermal changes to the sensitivity of ozone and related species to ENSO.

253

References

Bey, I., Jacob, D. J., Yantosca, R. M., Logan, J. A., Field, B. D., Fiore, A. M., Li, Q., Liu, H., Mickley, L. J., and Schultz, M. (2001), Global modeling of tropospheric chemistry with assimilated meteorology: Model description and evaluation, *J. Geophys. Res., 106*, 23,073-23,095.

Bjerknes, J., (1969), Atmospheric teleconnections from the equatorial Pacific, *Mon. Weather Rev.*, 18, 820-829.

Chandra, S., J. R. Ziemke, W. Min, et al. (1998), Effects of 1997-1998 El Niño on tropospheric ozone and water vapor, *Geophys. Res. Lett., 25*, 3867-3870.

Chandra, S., J. R. Ziemke, P. K. Bhartia, et al. (2002), Tropical tropospheric ozone: Implications for dynamics and biomass burning, *J. Geophys. Res.*, 107(D14), 4188, doi:10.1029/2001JD000447.

Chandra, S. J. R. Ziemke, B. N. Duncan, et al. (2009), Effects of the 2006 El Niño on tropospheric ozone and carbon monoxide: Implications for dynamics and biomass burning, *Atmos. Chem. Phys., 9*, 4239-4249.

Doherty, R. M., D. S. Stevenson, C. E. Johnson, W. J. Collins, and M. G. Sanderson (2006), Tropospheric ozone and El Niño–Southern Oscillation: Influence of atmospheric dynamics, biomass burning emissions, and future climate change , *J. Geophys. Res. , 111* , D19304, doi:10.1029/2005JD006849.

Duncan, B.N., S.E. Strahan, Y. Yoshida, S.D. Steenrod, and N. Livesey, (2007), Model Study of the Cross-Tropopause Transport of Biomass Burning Pollution, *Atmos. Chem. Phys., 7*, 3713-3736.

Enfield, D. B. (1989), El Niño, past and present, *Rev. Geophys., 27*(1), 159–187,

283   doi:10.1029/RG027i001p00159.

284 Jacobson, M. Z. (1995), Computation of global photochemistry with SMVGEAR II, *Atmos.*

285   *Environ., 29*, 2541–2546.

286 Kley, D., P. J. Crutzen, H. G. J. Smit, H. Vomel, S. J. Oltmans, H. Grassl, and V. Ramanathan

287   (1996), Observations of near-zero ozone concentrations over the convective Pacific:

288   Effects on air chemistry, *Science, 274*, 230–233.

289 Langford, A. O., T. J. O'Leary, C. D. Masters, K. C. Aikin, and M. H. Proffitt (1998), Modulation

290   of middle and upper tropospheric ozone at Northern midlatitudes by the El

291   Niño/Southern Oscillation, *Geophys. Res. Lett.*, 25, 2667-2670.

292 Langford, A. O. (1999), Stratosphere-troposphere exchange at the subtropical jet:

293   contribution to the tropospheric ozone budget at midlatitudes, *Geophys. Res. Lett.*, 26,

294   2449-2452.

295 Lee, S., D. M. Shelow, A. M. Thompson, and S. K. Miller (2010), QBO and ENSO variability in

296   temperature and ozone from SHADOZ, 1998–2005, *J. Geophys. Res., 115*, D18105,

297   doi:10.1029/2009JD013320.

298 Oort, A. H., and J. J. Yienger (1996), Observed interannual variability in the Hadley

299   circulation and its connection to ENSO, J. Clim., 9(11), 2751 – 2767.

300 Philander, S.G. (1989), El Niño, La Nina, and the Southern Oscillation, pp. 293. Academic

301   Press, San Diego, California, United States.

302 Quan, X.-W., H. F. Diaz, and M. P. Hoerling (2004), Change in the tropical Hadley cell since

303   1950, in The Hadley Circulation: Past, Present, and Future, edited by H. F. Diaz and R. S.

304   Bradley, Cambridge Univ. Press, New York.

305   Randel, W. J., and J. B. Cobb (1994), Coherent variations of monthly mean total ozone and

306   lower stratospheric temperature. *J. Geophys. Res.*, 99, 5433–5477.

307   Randel, W. J., and A. M. Thompson (2011), Interannual variability and trends in tropical

308   ozone derived from SAGE II satellite data and SHADOZ ozonesondes, *J. Geophys. Res.*,

309   *116*, D07303, doi:10.1029/2010JD015195.

310   Rayner, N. A., D. E. Parker, E. B. Horton, C. K. Folland, L. V. Alexander, D. P. Rowell, E. C. Kent,

311   and A. Kaplan (2003), Global analyses of sea surface temperature, sea ice, and night

312   marine air temperature since the late nineteenth century, *J. Geophys. Res.*, 108(D14),

313   4407, doi:10.1029/2002JD002670.

314   Rienecker, M.M., M.J. Suarez, R. Todling, J. Bacmeister, L. Takacs, H.-C. Liu, W. Gu, M.

315   Sienkiewicz, R.D. Koster,R. Gelaro, I. Stajner, and J.E. Nielsen (2008), The GEOS-5 Data

316   Assimilation System - Documentation of Versions 5.0.1, 5.1.0, and 5.2.0. *Technical*

317   *Report Series on Global Modeling and Data Assimilation*, 27.

318   Strahan, S.E., B.N. Duncan and P. Hoor (2007), Observationally-derived diagnostics of transport

319   in the lowermost stratosphere and their application to the GMI chemistry transport model,

320   *Atmos. Chem. Phys.*, 7, 2435-2445.

321   Sudo, K., M. Takahashi (2001), Simulation of tropospheric ozone changes during 1997-1998 El

322   Niño: Meteorological impact on tropospheric photochemistry, *Geophys. Res. Lett.*, 28, 4091-

323   4094.

324   Thompson, A. M., J. C. Witte, R. D. Hudson, et al. (2001), Tropical tropospheric ozone and

325   biomass burning, *Science, 291*, 2128-2182.

326   Thompson, A.M., J.C. Witte, R.D. McPeters, S.J. Oltmans, F.J. Schmidlin, J.A. Logan,

327   M.Fujiwara, V.W.J.H. Kirchhoff, F. Posny, G.J.R. Coetzee, B. Hoegger, S. Kawakami, T.

328 Ogawa, B.J. Johnson, H. Vömel and G. Labow (2003), Southern Hemisphere Additional

329 Ozonesondes (SHADOZ) 1998-2000 tropical ozone climatology 1. Comparison with

330 Total Ozone Mapping Spectrometer (TOMS) and ground-based measurements, *J.*

331 *Geophys. Res.*, Vol. 108 No. D2, 8238, doi: 10.1029/2001JD000967.

332 Voulgarakis, A., P. Hadjinicolaou, and J. A. Pyle (2011), Increases in global tropospheric

333 ozone following an El Niño event: examining stratospheric ozone variability as a

334 potential driver, *Atmos Sci. Let.*, 12, doi: 10.1002/asl.318

335 Zeng, G., and J. A. Pyle (2005), Influence of El Niño Southern Oscillation on

336 stratosphere/troposphere exchange and the global tropospheric ozone budget, *Geophys. Res.*

337 *Lett.*, 32, L0814, doi:10.1020/2004GL021353.

338 Ziemke, J. R., and S. Chandra (2003), La Nina and El Niño-induced variabilities of ozone in the

339 tropical lower atmosphere during 1970-2001, *Geophys. Res. Lett.*, *30*, 1142,

340 doi:10.1029/2002GL016387.

341 Ziemke, J. R., S. Chandra, B. N. Duncan, L. Froidevaux, P. K. Bhartia, P. F. Levelt, and J. W.
342 Waters (2006), Tropospheric ozone determined from Aura OMI and MLS: Evaluation of
343 measurements and comparison with the Global Modeling Initiative's Chemical
344 Transport Model, *J. Geophys. Res.*, *111*, D19303, doi:10.1029/2006JD007089.

345 Ziemke, J. R., S. Chandra, B. N. Duncan, M. R. Schoeberl, O. Torres, M. R. Damon, and P. K.
346 Bhartia (2009), Recent biomass burning in the tropics and related changes in
347 tropospheric ozone, *Geophys. Res. Lett.*, 36, L15819, doi:10.1029/2009GL039303.

348 Ziemke, J. R., S. Chandra, L. D. Oman, and P. K. Bhartia (2010), A new ENSO index derived

349 from satellite measurements of column ozone, *Atm. Chem. Phys.*, 10, 3711-3721.

350

351

352

353

354   Figure Captions

355   Figure 1. Comparison of the tropospheric column ozone sensitivity (DU/K) to the Niño 3.4

356   Index for a) 6 years of MLS/OMI measurements, b) 6 years of GEOS CCM simulation, c) 25

357   years of GEOS CCM simulation. Shaded regions are not significant at the 95% level. The

358   black rectangles show two regions used in calculating the Ozone ENSO Index.

359

360   Figure 2. Comparison of GEOS CCM simulation and *Ziemke et al.* [2010] measurement

361   derived Ozone ENSO Index (OEI) with Niño 3.4 Index (multiplied by 3) for the 1985 to

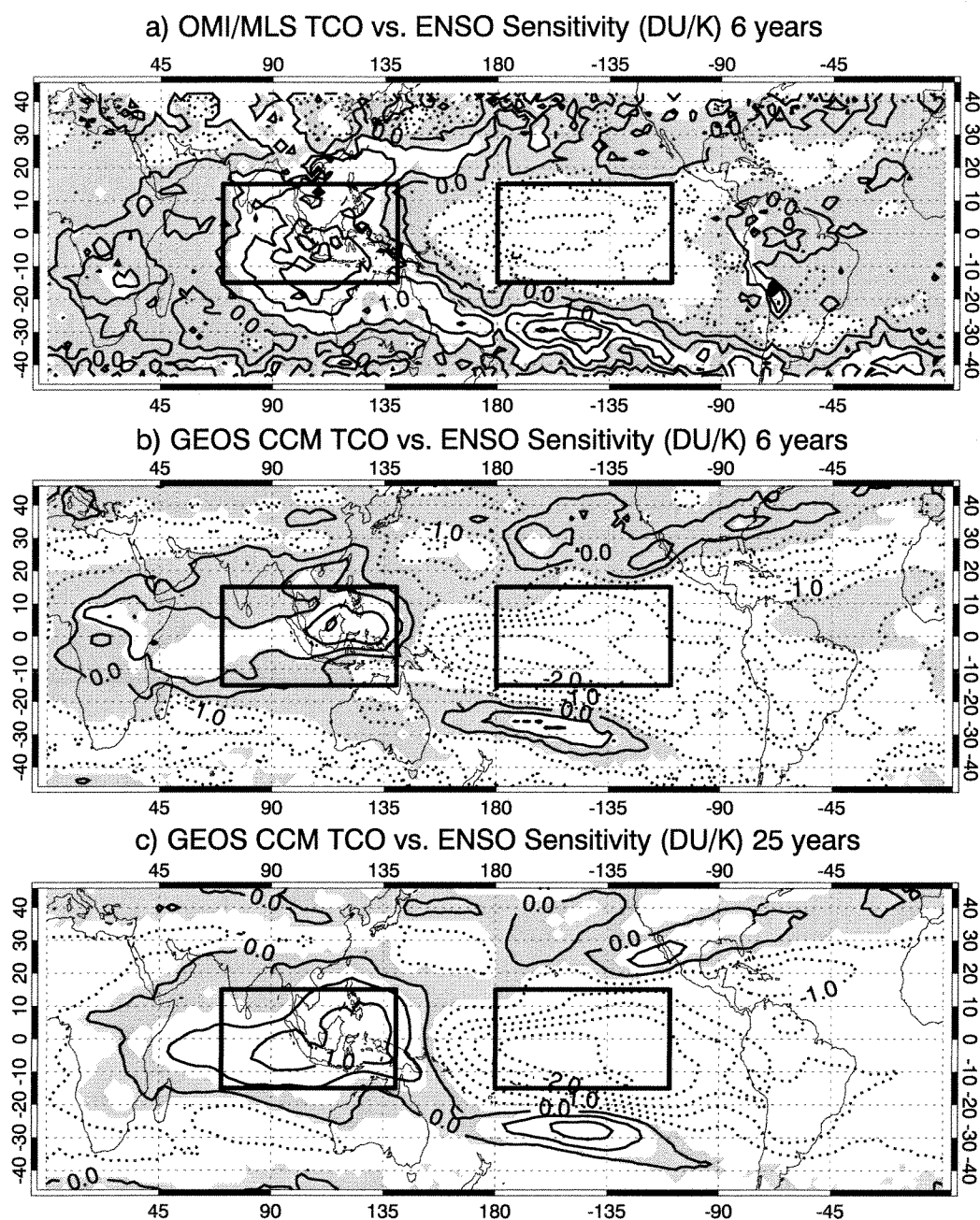362   2009 time period.

363

364   Figure 3. Sensitivity coefficient (ppbv/K) formed from linearly regressing deseasonalized

365   tropical (15°S-15°N, a), eastern region (180°W-110°W, b), and western region (70°E-

366   140°E, c) average ozone against Niño 3.4 Index. Overlaid is the anomalous circulation

367   shown by the streamfunction obtained by regressing the zonal wind and vertical velocity

368   (a), or meridional wind and vertical velocity (b,c) against Niño 3.4 Index. The dashed black

369   curve on all panels shows the mean model tropopause.

370

371   Figure 4. Vertical structure of ozone sensitivity (ppbv/K) to Niño 3.4 Index derived from

372   SHADOZ ozonesondes over the western (red diamonds) and eastern (blue diamonds)

373   regions of the tropical Pacific. GEOS CCM sensitivities sampled for the SHADOZ locations

374   are shown as solid curves.

375

376

377   Figures

a) OMI/MLS TCO vs. ENSO Sensitivity (DU/K) 6 years

b) GEOS CCM TCO vs. ENSO Sensitivity (DU/K) 6 years

c) GEOS CCM TCO vs. ENSO Sensitivity (DU/K) 25 years

378
379   Figure 1. Comparison of the tropospheric column ozone sensitivity (DU/K) to the Niño 3.4
380   Index for a) 6 years of MLS/OMI measurements, b) 6 years of GEOS CCM simulation, c) 25
381   years of GEOS CCM simulation. Shaded regions are not significant at the 95% level. The
382   black rectangles show two regions used in calculating the Ozone ENSO Index.
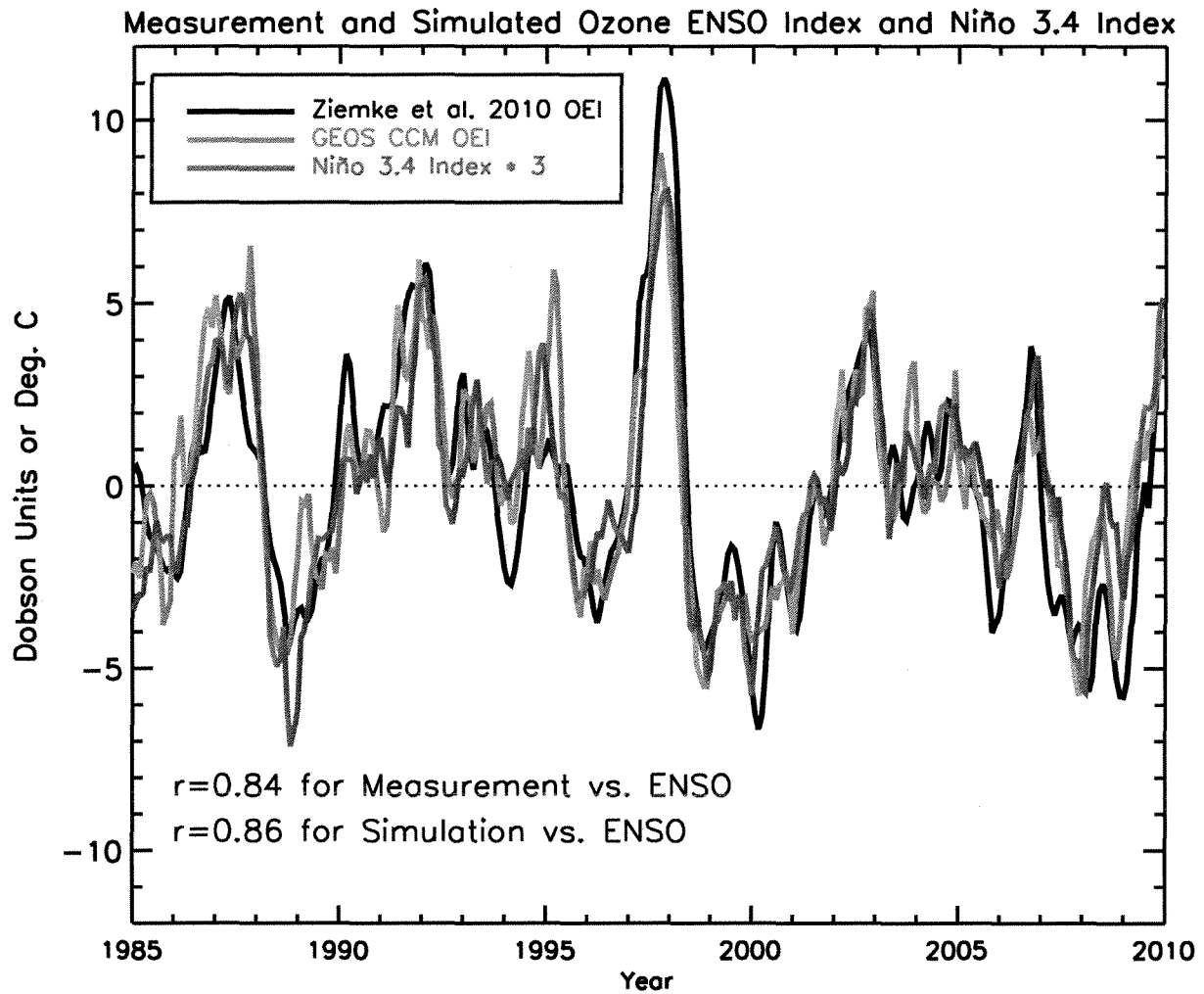
Figure 2. Comparison of GEOS CCM simulation and *Ziemke et al.* [2010] measurement
derived Ozone ENSO Index (OEI) with Niño 3.4 Index (multiplied by 3) for the 1985 to
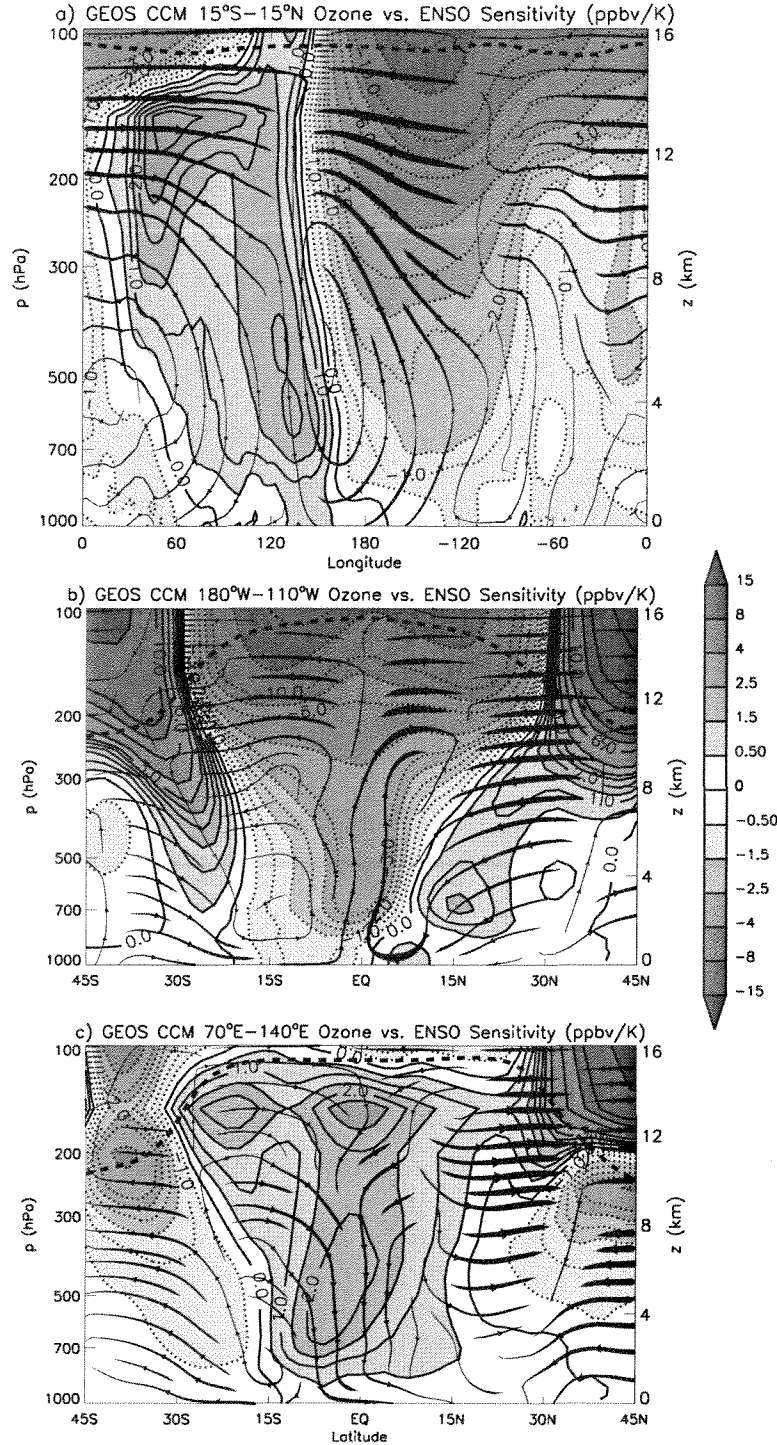2009 time period.

Figure 3. Sensitivity coefficient (ppbv/K) formed from linearly regressing deseasonalized tropical (15°S-15°N, a), eastern region (180°W-110°W, b), and western region (70°E-140°E, c) average ozone against Niño 3.4 Index. Overlaid is the anomalous circulation shown by the streamfunction obtained by regressing the zonal wind and vertical velocity (a), or meridional wind and vertical velocity (b,c) against Niño 3.4 Index. The dashed black curve on all panels shows the mean model tropopause.
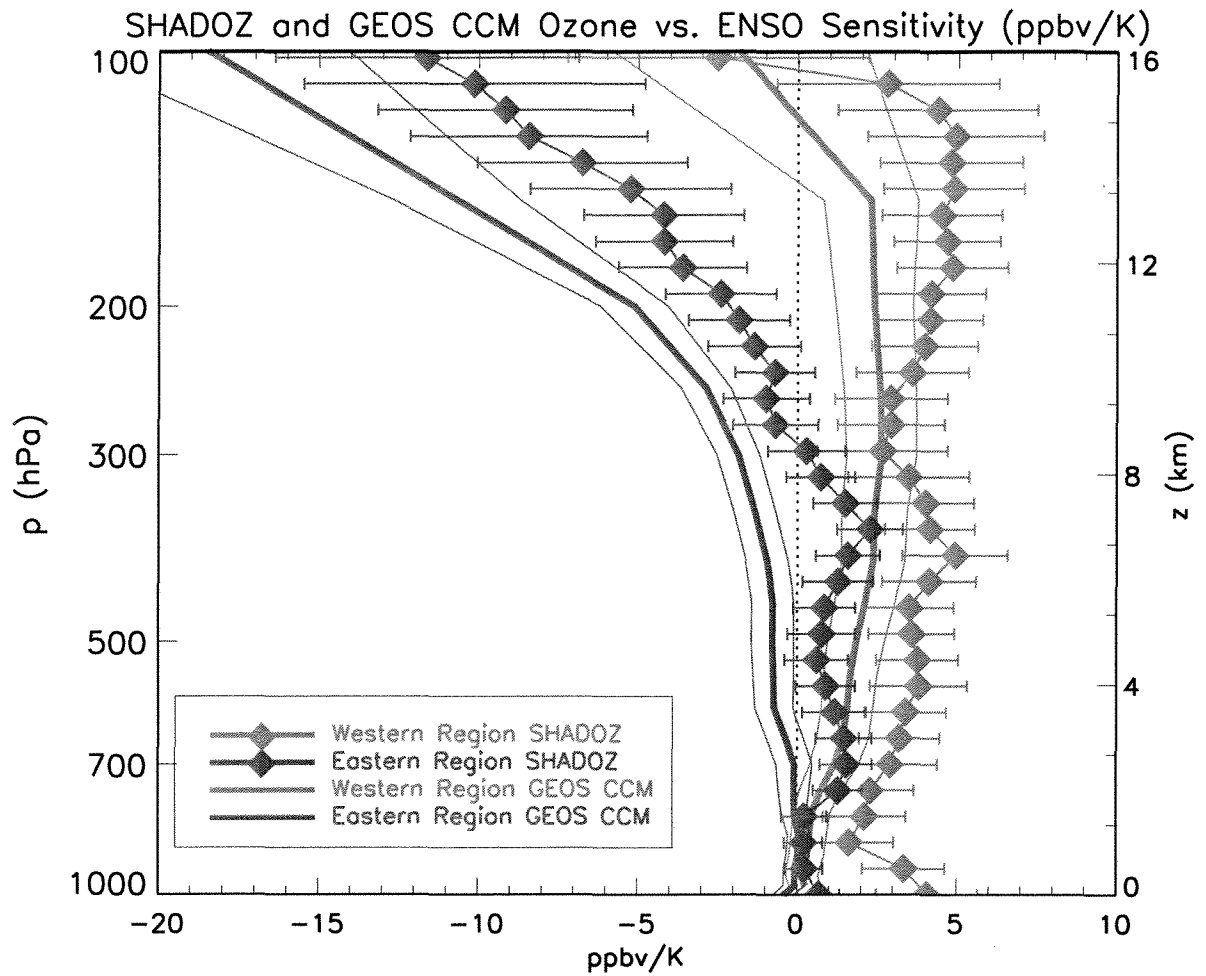
SHADOZ and GEOS CCM Ozone vs. ENSO Sensitivity (ppbv/K)

Western Region SHADOZ
Eastern Region SHADOZ
Western Region GEOS CCM
Eastern Region GEOS CCM

408
409
410   Figure 4. Vertical structure of ozone sensitivity (ppbv/K) to Niño 3.4 Index derived from
411   SHADOZ ozonesondes over the western (red diamonds) and eastern (blue diamonds)
412   regions of the tropical Pacific. GEOS CCM sensitivities sampled for the SHADOZ locations
413   are shown as the solid curves.
414
415
416
417
418
419
420
421
422
423
424
425